Electronic Structure of Dimanganese(II,III) and Dimanganese(III,IV) Complexes and Dimanganese Catalase Enzyme: A General EPR Spectral Simulation Approach

M. Zheng,[†] S. V. Khangulov,[†] G. C. Dismukes,*[,†] and V. V. Barynin[‡]

Henry H. Hoyt Laboratory, Department of Chemistry, Princeton University, Princeton, New Jersey 08544, and Institute of Crystallography, Russian Academy of Sciences, Moscow, Russia

Received October 27, 1993[⊗]

A general approach for simulation of EPR spectra of mixed-valence dimanganese complexes and proteins is presented, based on the theory of Sage et al. (*J. Am. Chem. Soc.* **1989**, *111*, 7239–7247), which overcomes limitations inherent in the theory of strongly coupled ions. This enables explanation of "anomalous" spectral parameters and extraction of accurate **g** tensors and ^{55}Mn magnetic hyperfine tensors from which the spatial distribution of the unpaired spin density, the electronic configuration, and ligand field parameters have been obtained. This is used to analyze highly accurate simulations of the EPR spectra, obtained by least-squares fits of two mixed valence oxidation states, from a series of dimanganese(II,III) and dimanganese(III,IV) complexes and from the dimanganese catalase enzyme, MnCat(II,III) and MnCat(III,IV), from *Thermus thermophilus*. The sign of the ^{55}Mn dipolar hyperfine anisotropy (Δa) reveals that the valence orbital configuration of the Mn(III) ion in MnCat(III,IV) and all dimanganese(III,IV) complexes possessing sterically unconstrained bis(μ-oxo) bridges is $d_x{}^3(d_{z^2})^1$, with the antibonding d_{z^2} electron oriented perpendicular to the plane of the $Mn_2(\mu\text{-}O)_2$ rhombus. This accounts for the strong Mn–O bonding and slow ligand exchange kinetics widely observed. The asymmetry of the spin density of Mn(III) increases substantially from $\Delta a/a_{iso} = 0.27$ in MnCat(III,IV) to 0.46 in MnCat(II,III), reflecting a change in manganese coordination. Comparison with model complexes suggest this may be due to protonation and opening of the $(\mu\text{-}O)_2$ bridge upon reduction to yield a single μ-OH bridge. The presence of strong Mn–O bonding in an unreactive $(\mu\text{-}O)_2$ core of MnCat(III,IV) offers a plausible explanation for the 10^{12} slower kinetics of peroxide dismutation compared to what is observed for the physiologically important oxidation state MnCat(II,II). For the dimanganese(II,III) oxidation state, the theory also provides the first explanation for the anomalously large (~30%) ^{55}Mn(II) hyperfine anisotropy in terms of admixing of the $S = {}^3/_2$ excited state into the ground state ($S = {}^1/_2$) via the zero-field splitting interaction of Mn(III). This "transferred" anisotropy obscures the otherwise typical isotropic high-spin $3d^5$ orbital configuration of Mn(II). An estimate of the ratio of the zero-field splitting to the Heisenberg exchange interaction (D/J) is obtained. The theory also explains the unusual 12-line EPR spectrum for a weakly coupled dimanganese(III,IV) complex (Larson et al. *J. Am. Chem. Soc.* **1992**, *114*, 6263–6265), in contrast to the typical 16-line "multiline" spectra seen in strongly coupled dimanganese(III,IV) complexes. The theory shows this is due to a weak $J = -10$ cm^{-1} which results in a D/J ratio approaching unity and not to unusual intrinsic magnetic hyperfine parameters of the Mn ions.

Introduction

EPR spectroscopy has been used for more than a decade to identify and distinguish the oxidation states of spin-coupled dimanganese(II,III) and (III,IV) complexes.[1-3] However, the theory used for EPR spectral interpretation has been restricted to the strong coupling case where the Heisenberg–Dirac–Van Vleck (HDVV) exchange interaction between Mn ions is much stronger than the zero-field splitting originating from both spin–orbital and dipolar interactions ($|J| \gg |D|$). This condition is usually met for dimanganese(III,IV) complexes for which the ground doublet state is usually well isolated from excited spin states with $S > {}^1/_2$. However, for dimanganese(II,III) complexes, the exchange interactions are typically weak,[3] and evidence is emerging[4] that not all dimanganese(III,IV) systems fall into the strong coupling category. For these complexes analysis of the EPR spectra via simulations has either not been reported or predicts anomalous magnetic parameters for the Mn ions which are unprecedented and have not been explained. Hence it is necessary to extend the existing theory in order to interpret experimental spectra from a wider range of complexes.

Another issue which has been widely ignored in EPR spectral simulations is the highly anisotropic nature of ^{55}Mn(III) hyperfine interactions (but see ref 5a). This originates from the asymmetry in the electron spin density of the $3d^4$ valence orbital configuration. Because of this neglect, determination of the valence orbital configuration from analysis of the Mn(III) hyperfine anisotropy has not been explored for most Mn(III)-containing complexes. In octahedral ligand fields, the high-spin $3d^4$ orbital configuration of Mn(III) undergoes spontaneous distortion in which the single d_σ antibonding electron may be localized in either the d_{z^2} orbital, yielding a tetragonal expansion, or the $d_{x^2-y^2}$ orbital, yielding a tetragonal compression. This coupling of electron–nuclear motion, termed the Jahn–Teller interaction, leads to major differences in the bonding strength, kinetic lability and chemical reactivity of the axial and equatorial ligands (relative to the d_σ orbital). For example, the activation barrier to rotation of the tetragonal distortion from one bond axis to another is a direct measure of the nuclear–electronic coupling energy. In MnF_6^{3-}, for example, this barrier is very large at $E_a \sim 3500$ cm^{-1},[6] with

[†] Princeton University.
[‡] Russian Academy of Sciences.
[⊗] Abstract published in *Advance ACS Abstracts*, December 15, 1993.

(1) Cooper, S. R.; Dismukes, G. C.; Klein, M. P.; Calvin, M. *J. Am. Chem. Soc.* **1978**, *100*, 7248–7252.
(2) Dismukes, G. C.; Sheats, J. E.; Smegal, J. A. *J. Am. Chem. Soc.* **1987**, *109*, 7202–7203.
(3) Diril, H.; Chang, H. R.; Nilges, M. J.; Zhang, X.; Potenza, J. A.; Schugar, H. J.; Isied, S. S.; Hendrickson, D. N. *J. Am. Chem. Soc.* **1989**, *111*, 5102–5114.
(4) Larson, E.; Haddy, A.; Kirk, M. L.; Sands, R. H.; Hatfield, W. E.; Pecoraro, V. L. *J. Am. Chem. Soc.* **1992**, *114*, 6263–6265.
(5) (a) Vanngard, T.; Hansson, O.; Haddy, A. In *Manganese Redox Enzymes*; Pecoraro, V. L., Ed.; VCH: New York, 1992; pp 105–118. (b) Fronko, R. M.; Penner-Hahn, J. E. *J. Am. Chem. Soc.* **1988**, *110*, 7554–7555.

0020-1669/94/1333-0382$04.50/0

comparable coupling energies expected for O^{2-} and OH^- ligands. This kinetic barrier may actually become rate-limiting to the kinetics of intracluster electron transfer and also substrate binding and product release in manganoenzymes. As we will show it is possible to distinguish these two orbital configurations from the sign of the ^{55}Mn hyperfine anisotropy determined from EPR spectroscopy.

In this study, several examples of highly anisotropic EPR spectra from mixed valence dimanganese complexes and the catalase enzyme from *Thermus thermophilus* are accurately simulated using a nonlinear least-squares fitting procedure. From the simulated spectra we obtain the intrinsic ^{55}Mn hyperfine tensor of each Mn ion, which enables assignment of the oxidation state and electronic orbital configuration of Mn(III). The ^{55}Mn magnetic hyperfine tensor so obtained and the intermanganese HDVV exchange interaction, deduced from the EPR temperature dependence, allow us to separate the hyperfine anisotropy arising from orbital spatial asymmetry (i.e., dipolar), from that due to "transferred" zero-field splitting arising from admixing with low-lying spin states. We find that the latter case explains the large hyperfine anisotropy of most Mn(II) ions in dimanganese(II,III) complexes, while the former case explains the large hyperfine anisotropy of the Mn(III) ions in the majority of dimanganese-(III,IV) complexes. A substantial increase in magnitude of the hyperfine anisotropy of Mn(III) from MnCat(III,IV) to MnCat-(II,III) leads us to the conclusion that there is a ligand field change upon reduction. The MnCat(II,III) EPR simulation offers positive identification of the first example of the mixed-valence dimanganese(II,III) oxidation state in any biological system.

It is also our hope that by illustrating the method for obtaining the molecular electronic parameters from the spectroscopic parameters derived from simulations, we can provide a structural basis for the different chemical reactivities of these oxidation states.

Experimental Section

Sample Preparation and EPR Spectroscopy. $[Mn_2(bipy)_4(\mu\text{-}O)_2](ClO_4)_3\cdot 2H_2O$ (**1**), was prepared as previously described.[1] A frozen solution of **1** in spectrograde acetonitrile was prepared in a cylindrical quartz tube for EPR measurements.[1]

$[Mn_2O(OAc)_2(HB(pz)_3)_2]$, where $HB(pz)_3$- is hydrotris(1-pyrazolyl)-borate, was prepared and oxidized by $KMnO_4$ in a two-phase aqueous methylene chloride mixture.[7] The dimanganese(III,IV) oxidation product **2** is formulated as the neutral bis(μ-oxo)–carboxylato-bridged complex $[Mn_2O_2(OAc)(HB(pz)_3)_2]$, according to EPR (antiferromagnetic exchange coupling ($|J| > 150$ cm^{-1}) and resonance Raman spectroscopy (ν_s = 705 cm^{-1}, 676 (^{18}O) cm^{-1}; five of the eight predicted vibrational modes of the planar Mn_2O_2 rhombus downshift upon exchange $^{16}O \rightarrow {}^{18}O$; Czernuszewicz, Sheats, and Dismukes, unpublished).[7]

The preparation and EPR measurements of MnCat(II,III) and MnCat-(III,IV) from *T. thermophilus* are described in ref 8d.

EPR Spectral Simulations. The spin hamiltonian for a spin-coupled dimer was solved to second order in perturbation theory.[1] The parameters used for simulation are two hyperfine tensors, one **g** tensor, their Euler angles and a Lorentzian line width. The line width of all transitions was assumed to be independent of orientation and of the ^{55}Mn nuclear state. This is an important simplification over previous simulations which employed large orientation-dependent line widths for dimanganese(II,III) complexes varying by 5-fold[3] or nuclear state dependent (m_I) line widths.[1] Simulation is done first by a trial-and-error method until approximate agreement between the experimental and the simulated spectra is achieved. These parameters are then used as the initial guess in a nonlinear least-squares fitting program called MRQMIN.[9] In this procedure, the difference between the simulated spectrum (Y_s) and the experimental one (Y_e) is measured by

$$\chi^2 = \sum_{i=1}^{m} (Y_s(i) - Y_e(i))^2$$

which is a function of the fitting parameters. The program calculates the value of χ^2 and the slope at the present point in the multidimensional parameter space and minimizes χ^2, iteratively. The minimization is stopped when

$$R = \frac{\chi^2}{\sum_{i=1}^{m} Y_e(i)^2}$$

is converged to a global minimum, which can usually be achieved after about 20 iterations. The route to the global minimum can also be controlled manually by fixing certain parameters, while letting others vary. All of the simulation were performed on a DEC Vax 3400 computer having 24 Mbyte memory. A typical run takes about 1 h of CPU time.

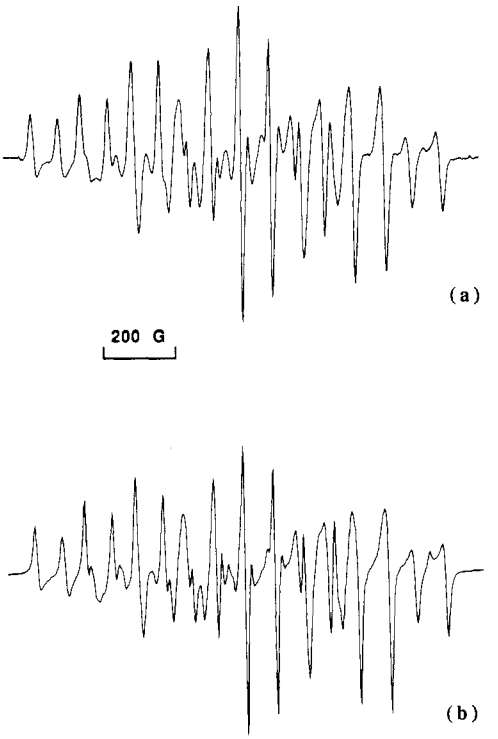

Figure 1. EPR spectra of the manganese catalase(III,IV) oxidation state at 9.38 GHz and 15 K: (a) Experimental; (b) simulation.

Results

To illustrate the quality of the spectral fits, simulations of the EPR spectra of MnCat(III,IV) and MnCat(II,III) from *T. thermophilus* are compared to the corresponding experimental spectra in Figures 1 and 2, respectively. The best fit parameters and R values are summarized in Tables 1a and 2a. In all the cases, we have assumed that the hyperfine and **g** tensors are colinear. We found that although axial **g** and hyperfine tensors can produce most spectral features, incorporation of a small rhombicity in both the hyperfine and **g** tensors improves the R value by 1–2-fold, so that virtually all of the detailed spectral features can be reproduced.

The EPR spectrum of the MnCat(III,IV) oxidation state from the enzyme isolated from *Lactobacillus plantarum* also exhibits

(6) Englman, R. *The Jahn-Teller Effect in Molecules and Crystals*; Wiley-Interscience: London, 1972; p 322.
(7) Sheats, J. E.; Czernuszewicz, R. S.; Dismukes, G. C.; Rheingold, A. L.; Petrouleas, V.; Stubbe, J.; Armstrong, W. H.; Beer, R. H.; Lippard, S. J. *J. Am. Chem. Soc.* **1987**, *109*, 1435–1444.
(8) (a) Barynin, V. V.; Vagin, A. A.; Melik-Adamyan, W. R.; Grebenko, A. I.; Khangulov, S. V.; Popov, A. N.; Andriyanova, M. E. *Dokl. Acad. Nauk SSSR* **1986**, *288*, 877–880. (b) Khangulov, S. V.; Barynin, V. V.; Melik-Adamyan, V. R.; Grebenko, A. I.; Voevodskaya, N. V.; Blumenfeld, L. A.; Dobryakov, S. N.; Ilyasova, V. B. *Bioorg. Khim.* **1986**, *12*, 741–748. (c) Khangulov, S. V.; Barynin, V. V.; Voevodskaya, N. V.; Grebenko, A. I. *Biochim. Biophys. Acta* **1990**, *1020*, 305–310. (d) Khangulov, S. V.; Barynin, V. V.; Autonyuk-Barynina, S. V. *Biochim. Biophys. Acta* **1990**, *1020*, 25–33.
(9) Press, W. H.; Flannery, B. P.; Tenkolsky, S. A.; Vetterling, W. T. *Numerical Recipes (FORTRAN Version)*; Cambridge University Press: Cambridge, England, 1989; pp 521–528.

Table 1. Parameters for Dimanganese(III,IV) Complexes

(a) Simulation Parameters[a] Used for Dimanganese(III,IV) Spectra [(A_x, A_y, A_z): effective hyperfine tensor (MHz)]

	Mn(III) (A_x, A_y, A_z)	Mn(IV) (A_x, A_y, A_z)	(g_x, g_y, g_z)	R/%
complex **1**	(−483, −498, −378)	(214, 211, 231)	(1.992, 1.998, 1.982)	1.0
complex **2**	(−436, −474, −326)	(226, 213, 235)	(2.001, 2.002, 1.985)	3.5
MnCat(III,IV)	(−410, −425, −315)	(235, 224, 252)	(2.014, 2.014, 2.000)	4.5
MnCat(III,IV)[b]	(−420, −420, −305)	(225, 225, 249)	(2.008, 2.008, 1.993)	NA

(b) Intrinsic ^{55}Mn Hyperfine Parameters for Mn(III) (MHz) and Correlation of Ligand Set with EPR Line Width in Dimanganese(III,IV) Complexes

	ligand type	ΔH/G	(a_x, a_z)	a_{iso}	Δa
complex **1**	2O, 4N	14.0	(−245, −189)	−227	56
complex **2**	3O, 3N	9.2	(−228, −163)	−206	65
MnCat(III,IV)	6O or 5O, N[c]	7.9	(−209, −157)	−192	52

[a] Simulation can provide only the magnitude of hyperfine tensor elements. But since it is known that the intrinsic hyperfine values for Mn ions are negative in sign, we are able to determine the sign of hyperfine tensor elements as listed here. Complex **1** = $[Mn_2(bipy)_4(\mu\text{-}O)_2](ClO_4)_3\cdot 2H_2O$; complex **2** = $[Mn_2O_2(OAc)(HB(pz)_3)_2]$, where $HB(pz)_3$- is hydrotris(1-pyrazolyl)borate. [b] Data from ref 5a for MnCat from *Lactobacillus plantarum*. [c] Data from ref 15.

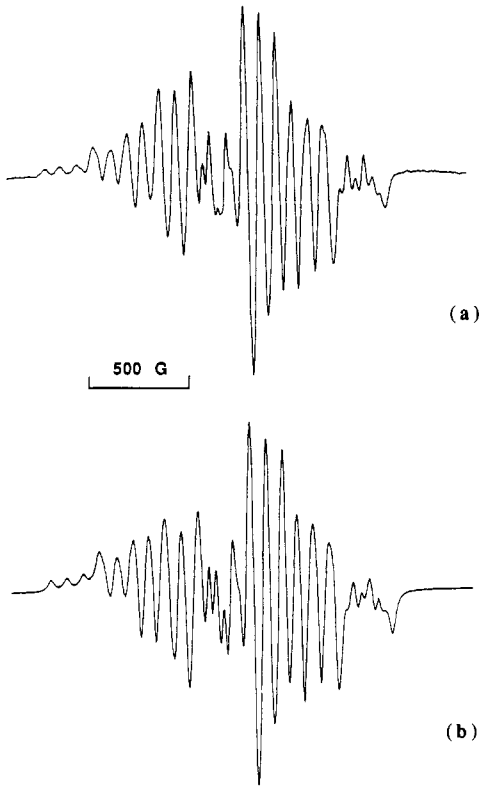

Figure 2. EPR spectrum of the manganese catalase(II,III) oxidation state at 9.38 GHz and 15 K: (a) experimental; (b) simulation.

a similar 16-line spectrum, but no spectrum corresponding to the MnCat(II,III) oxidation state has been reported as yet.[5] Simulation parameters for MnCat(III,IV) from *L. plantarum* are included in Table 1a for comparison.[5] Table 2a also includes for comparison parameters reported in ref 3 from simulations of the EPR spectra in frozen glasses of the manganese(II,III) compounds $[Mn_2(bcmp)(\mu\text{-}OAc)_2](ClO_4)_2\cdot CH_2Cl_2$ (**3**) and $[Mn_2(bpmp)(\mu\text{-}OAc)_2](ClO_4)_2\cdot H_2O$ (**4**), where bcmp$^-$ is the monoanion of 2,6-bis(1,4,7-triazacyclonon-1-ylmethyl)-4-methylphenol, and bpmp$^-$ is the monoanion of 2,6-bis[bis(2-pyridylmethyl)aminomethyl]-4-methylphenol. In each of these compounds the two Mn atoms are bridged by two bidentate acetate ions and by the phenoxide O atom of the bcmp$^-$ and bpmp$^-$ ligands. The Mn ions in both complexes possess pseudooctahedral coordination and the Mn(III) ion is Jahn–Teller distorted by elongation along one direction according to X-ray analysis.[3] For example, the structural data of **4** reveals that the axial Mn–N bond is 0.17 Å longer than the equatorial Mn–N bonds, and the axial Mn–O bond is 0.18 Å longer than the equatorial Mn–O bonds. The similarity of the three sets of data in Table 2a and the difference with those listed in the Table 1a are easy to see. Thus, the assignments of the catalase EPR spectra to the mixed-valence dimanganese(II,III) and dimanganese(III,IV) oxidation states can be made with confidence. Previous predictions were based solely on qualitative comparisons to model complexes rather than simulations.[8]

Discussion

To go beyond using the EPR spectra merely to identify the manganese oxidation states, we explore next the physical meaning of the observed hyperfine tensors. For the convenience of our discussion, we summarize in the following section data found in the literature for the intrinsic hyperfine tensors of monomeric Mn(II), Mn(III), and Mn(IV) complexes, along with the applicable zero-field splitting parameters. A theoretical discussion of the Mn(III) hyperfine anisotropy needed for interpretation of our data is also included.

Mn(II) and Mn(IV). Consistent with the symmetrical electronic configurations of Mn(II) (d^5 half-filled shell) and Mn(IV) (t_{2g}^3 half-filled shell in an octahedral ligand field), the observed magnetic hyperfine tensors for these ions in a variety of monomeric complexes are nearly isotropic, with values ranging from 90 to 60 G, respectively.[10] In addition, the zero-field splittings for Mn(II) and Mn(IV) ions are typically small ($|D| \leq 10^{-1}$ cm^{-1}) compared with the range of exchange interactions encountered in mixed-valence dimanganese complexes ($|J| \geq 10^0$ cm^{-1}).[10]

Mn(III). EPR from Mn(III) ions is not easy to observe, because the 5-fold spin degeneracy of the high-spin $S = 2$ state is lifted by the combined effects of spin–orbit coupling and the electrostatic ligand field. Consequently, experimental data on the hyperfine tensor are rare.[5,11] An anisotropic hyperfine tensor with principal values $a_x = a_y = -84.5 \times 10^{-4}$ cm^{-1} (−253.5 MHz) and $a_z = -52.8 \times 10^{-4}$ cm^{-1} (−158.4 MHz) was reported for Mn(III) in the octahedral rutile (TiO_2) lattice. The experimental data were analyzed within the framework of crystal field theory, using eq 1.[11] The "+" and "−" signs apply to the $d_{xy}^1d_{yz}^1d_{zx}^1d_{z^2}^1$ and

$$\Delta a = a_z - a_x = \pm\frac{3}{14}g_e\beta_e g_I\beta_I\langle r^{-3}\rangle \qquad (1)$$

$d_{xy}^1d_{yz}^1d_{zx}^1d_{x^2-y^2}^1$ configurations, respectively. For Mn(III) ions in the gas phase $\langle r^{-3}\rangle$ is calculated to be 4.7 (au) which gives $|\Delta a| = 130$ MHz.[11] For Mn(III) in condensed phases $\langle r^{-3}\rangle$ is invariably

(10) (a) Reed, G. H.; Markham, G. D. In *Biological Magnetic Resonance*; Berliner, L. J., Reuben, J., Eds.; Plenum: New York, 1984; Vol. 6, pp 73–142. (b) Andresen, H. G. *Phys. Rev.* **1960**, *120*, 1606–1611. (c) Geschwind, S.; Kisliuk, P.; Klein, M. P.; Remeika, J. P.; Wood, D. L. *Phys. Rev.* **1962**, *126*, 1684–1686.
(11) Gerritsen, H. J.; Sabisky, E. S. *Phys. Rev.* **1963**, *132*, 1485–1512.
(12) Kennedy, B. J.; Murray, K. S. *Inorg. Chem.* **1985**, *24*, 1552–1557.

Table 2. Parameters for Dimanganese(II,III) Complexes

(a) Simulation Parameters Used for Dimanganese(II,III) Spectra [(A_x, A_y, A_z): effective hyperfine tensor (MHz)]

	Mn(II) (A_x, A_y, A_z)	Mn(III) (A_x, A_y, A_z)	(g_x, g_y, g_z)	R/%
MnCat(II,III)	(−529, −502, −730)	(222, 210, 236)	(1.958, 1.965, 2.025)	3.6
complex **3**[a]	(−459, −459, −735)	(219, 219, 318)	(1.905, 1.905, 2.022)	NA
complex **4**[a]	(−435, −435, −801)	(195, 195, 339)	(1.813, 1.883, 2.026)	NA

(b) Deduced Intrinsic Hyperfine Parameters (MHz) and Zero-Field Splitting Constants for Mn(II) and Mn(III) in Dimanganese(II,III) Systems[b]

	Mn(II)	Mn(III)				
	a_{iso}	(a_x, a_z)	a_{iso}	Δa	D/J	D/cm^{-1}
MnCat(II,III)	−253	(−207, −124)	−179	83	0.47	<0
complex **3**	−236	(−233, −150)	−205	83	0.63	−4.9
complex **4**	−239	(−237, −144)	−206	93	0.82	−4.9

[a] Data from ref 3. Complex **3** = $[Mn_2(bcmp)(\mu\text{-}OAc)_2](ClO_4)_2{\cdot}CH_2Cl_2$, where bcmp$^-$ is the monoanion of 2,6-bis(1,4,7-triazacyclonon-1-ylmethyl)-4-methylphenol; complex **4** = $[Mn_2(bpmp)(\mu\text{-}OAc)_2](ClO_4)_2{\cdot}H_2O$, where bpmp$^-$ is the monoanion of 2,6-bis[bis(2-pyridylmethyl)aminomethyl]-4-methylphenol. [b] In this work we have used formula from ref 13b to evaluate the intrinsic magnetic parameters of Mn ions. In ref 13c, a seemingly more rigorous solution was obtained for the same problem by solving exactly the spin Hamiltonian in a subspace spanned by $S = {}^1/_2$ and ${}^3/_2$ states. We found the two approaches give similar results. For instance D/J for MnCat(II,III) is estimated to be 0.5 by ref 13c's formulas, which is very close to the value of 0.47 estimated by ref 13b's method.

substantially reduced due to ligand covalency, and hence smaller hyperfine anisotropy would be expected.

In addition to this, for tetragonally distorted Mn(III) ions, the zero-field splitting parameter D is predicted to be positive for the $d_{xy}{}^1d_{yz}{}^1d_{zx}{}^1d_{x^2-y^2}{}^1$ configuration and negative for the $d_{xy}{}^1d_{yz}{}^1d_{zx}{}^1d_{z^2}{}^1$ configuration; $|D|$ was estimated to be ~ 5 cm^{-1} for Mn(III) in rutile.[11] This value is consistent with the range of $|D|$ values, 1–4 cm^{-1}, reported for a series of Mn(III) Schiff-base complexes.[12]

Spin Hamiltonian. The large zero-field splitting of Mn(III) has to be taken into account in the description of the ground-state properties of mixed-valence complexes when the HDVV exchange interaction is not so strong. Weak coupling is the usual case for dimanganese(II,III) complexes, but is rare for dimanganese(III,IV) complexes with one or more μ-monoatomic bridges. The latter are typically strongly coupled, except in a few cases.[4]

A general theory needed to describe the magnetic properties of $S = {}^1/_2$ mixed-valence complexes has been derived and applied to iron(II,III) complexes.[13] Here we apply this theory to consider weakly coupled dimanganese(II,III) complexes.

A spin Hamiltonian for an exchange coupled system with individual spins S_A and S_B ($S_A = S_B + {}^1/_2$), including zero-field splitting terms for each iron is given in eq 2. As a zero-order

$$\mathbf{H} = -2J\mathbf{S}_A\mathbf{S}_B + \mathbf{S}_A\mathbf{D}_A\mathbf{S}_A + \mathbf{S}_B\mathbf{D}_B\mathbf{S}_B + \mathbf{S}_A\mathbf{a}_A\mathbf{I}_A + \mathbf{S}_B\mathbf{a}_B\mathbf{I}_B + \mathbf{S}_A\mathbf{g}_A\mathbf{H} + \beta\mathbf{S}_B\mathbf{g}_B\mathbf{H} \quad (2)$$

approximation that corresponds to the strong coupling limit, the eigenstates of the antiferromagnetically coupled spin system will be grouped according to the total spin $S_T = {}^1/_2, {}^3/_2, \ldots$, with $S_T = {}^1/_2$ being the ground doublet. When finite zero-field splitting terms are present, matrix elements such as $\langle {}^3/_2,{}^1/_2|\mathbf{S}_i\mathbf{D}_i\mathbf{S}_i|{}^1/_2,{}^1/_2\rangle$, $\langle {}^3/_2,{}^{-1}/_2|\mathbf{S}_i|\mathbf{D}_i|\mathbf{S}_i|{}^1/_2,{}^{-1}/_2\rangle$, where i = A or B, have nonvanishing values. These cause mixing of the $|{}^3/_2,\pm{}^1/_2\rangle$ and other high level states into the zero-order ground doublet $|{}^1/_2,\pm{}^1/_2\rangle$. This can be treated as a first-order perturbation on the total spin functions, yielding eq 3 for the Zeeman and hyperfine interactions,[13] where

$$\mathbf{S}_A\mathbf{a}_A\mathbf{I}_A + \mathbf{S}_B\mathbf{a}_B\mathbf{I}_B + \mathbf{S}_A\mathbf{g}_A\mathbf{H} + \beta\mathbf{S}_B\mathbf{g}_B\mathbf{H} = \beta\mathbf{S}_T\mathbf{g}\mathbf{H} + \mathbf{S}_T\mathbf{A}_A\mathbf{I}_A + \mathbf{S}_T\mathbf{A}_B\mathbf{I}_B \quad (3)$$

$\mathbf{g}$, $\mathbf{A}_A$, $\mathbf{A}_B$ are defined by eq 3a–c, respectively. Here, $\mathbf{g}_A$, $\mathbf{g}_B$, $\mathbf{A}_A$, $\mathbf{A}_B$, $\mathbf{a}_A$, $\mathbf{a}_B$, $\mathbf{D}_A$, $\mathbf{D}_B$ are 3 × 3 matrices, while b_A, b_B and p_A, p_B

$$\mathbf{g} = p_A\mathbf{g}_A + p_B\mathbf{g}_B + (1/5)p_Ap_B(\mathbf{g}_A - \mathbf{g}_B)(b_A\mathbf{D}_A - b_B\mathbf{D}_B)/J \quad (3a)$$

$$\mathbf{A}_A = p_A\mathbf{a}_A - (1/5)p_Ap_B\mathbf{a}_A(b_A\mathbf{D}_A - b_B\mathbf{D}_B)/J \quad (3b)$$

$$\mathbf{A}_B = p_B\mathbf{a}_B + (1/5)p_Ap_B\mathbf{a}_B(b_A\mathbf{D}_A - b_B\mathbf{D}_B)/J \quad (3c)$$

are scalars defined as follows:

$$b_A = 3p_A + 1$$

$$b_B = 3p_B + 1$$

$$p_A = \frac{S_T(S_T+1) + S_A(S_A+1) - S_B(S_B+1)}{2S_T(S_T+1)}$$

$$p_B = \frac{S_T(S_T+1) + S_B(S_B+1) - S_A(S_A+1)}{2S_T(S_T+1)}$$

The first terms of eq 3a–c are the usual strong coupling terms; p_i's are actually the spin projections of each individual spin onto the total spin in the strong coupling limit.

Strong Coupling Case ($|D/J| \ll 1$). For dimanganese(III,IV) eq 3b,c become

$$\mathbf{A}_{III} = \mathbf{2a}_{III} + \frac{2}{5J}(7\mathbf{D}_{III} + 2\mathbf{D}_{IV})\mathbf{a}_{III} \quad (4)$$

$$\mathbf{A}_{IV} = -\mathbf{a}_{IV} - \frac{2}{5J}(7\mathbf{D}_{III} + 2\mathbf{D}_{IV})\mathbf{a}_{IV} \quad (5)$$

For complex **1** listed in Table 1, $J = -150$ cm^{-1} (yielding a quartet–doublet splitting of $\Delta E = 3J$),[1] while for complex **2** and MnCat(III,IV), J has been estimated from the temperature dependence of the EPR signals to be at least as large as that for complex **1**.[7,8b,c] To explain the hyperfine tensors listed in Table 1a, we may initially assume that the intrinsic hyperfine tensor for monomeric Mn(IV) is isotropic with $\mathbf{a}_{IV} = -220$ Mhz and $\mathbf{D}_{IV} = 0$. We may then estimate the contribution of the correction term in eq 5 to the Mn(IV) anisotropy originating from zero-field splitting of Mn(III). For an axial ZFS tensor $\mathbf{D}_{III}$ (with principal value equal to $D[S_z^2 - {}^1/_3S(S+1)]$) with magnitude −4 cm^{-1} and $J = -150$ cm^{-1}, the Mn(IV) anisotropy is

$$\Delta A_{IV} = A_{IV}(z) - A_{IV}(x) = -\frac{14a_{IV}D}{5J} = 16 \text{ MHz} \quad (6)$$

This has the same sign and a comparable magnitude to the experimentally observed Mn(IV) hyperfine anisotropy for the four dimanganese(III,IV) examples listed in Table 1a. Although

(13) (a) Valentine, M. *Hyperfine Interact.* **1986**, *30*, 309–335. (b) Sage, J. T.; Xia, Y.-M.; Debrunner, P. G.; Keough, D. T.; de Jersey, J.; Zerner, B. *J. Am. Chem. Soc.* **1989**, *111*, 7239–7247. (c) Bertrand, P.; Guigliarelli, B.; More, C. *New J. Chem.* **1991**, *15*, 445–454. (d) Guigliarelli, B.; Bertrand, P.; Gayda, J.-P. *J. Chem. Phys.* **1986**, *85*, 1689–1692.

there will also be a small direct dipolar source for the observed Mn(IV) hyperfine anisotropy, the "transferred" zero-field splitting perturbation is a major source which cannot be neglected.

For Mn(III) a similar estimation can be made, which shows that the contribution from the correction term in eq 4, originating from transferred zero-field splitting of Mn(IV), constitutes only a small part of the total hyperfine anisotropy observed. Therefore, the hyperfine anisotropy of Mn(III) is mainly determined by the intrinsic Mn(III) magnetic hyperfine anisotropy. Equation 4 gives $\mathbf{A}_{III} = 2\mathbf{a}_{III}$ as a first-order approximation to the observed effective hyperfine tensors listed in Table 1a. The deduced intrinsic hyperfine tensors are listed in Table 1b. For simplicity we have used an axial tensor here by taking the average of x and y components as the perpendicular component.

The first thing to notice is the positive sign of the hyperfine anisotropy for all four complexes. This clearly indicates that the electronic configuration of Mn(III) in all cases is predominantly $d_{xy}^1 d_{yz}^1 d_{zx}^1 d_{z^2}^1$. In the case of complex **1** this conclusion is consistent with the X-ray diffraction data showing elongated N–Mn–N axial bond lengths (0.138 Å longer than the equatorial Mn–N bonds) at the Mn(III) site perpendicular to the two short μ-O–Mn bonds.[14]

Intermediate Coupling Case ($|D/J| < 1$). For dimanganese(II,III) complexes, eq 3b,c becomes

$$\mathbf{A}_{II} = \frac{7}{3}\mathbf{a}_{II} + \frac{28}{45J}(8\mathbf{D}_{II} + 3\mathbf{D}_{III})\mathbf{a}_{II} \quad (7)$$

$$\mathbf{A}_{III} = -\frac{4}{3}\mathbf{a}_{III} - \frac{28}{45J}(8\mathbf{D}_{II} + 3\mathbf{D}_{III})\mathbf{a}_{III} \quad (8)$$

The HDVV exchange constants for complexes **3** and **4** were previously determined by magnetic susceptibility measurement to be $J = -7.7$ and -6.0 cm^{-1}, respectively.[3] For MnCat(II,III), the strong temperature dependence of the EPR line width broadening indicates a very weak exchange coupling.[8a,c] Although the exact value is not known, it can be estimated to be less than $J < -20$ cm^{-1}. For all of these cases, eqs 7 and 8 predict a substantial perturbation from zero-field splitting on the effective hyperfine tensors. If we assume that the observed hyperfine anisotropy for Mn(II) in catalase is determined solely by the transferred zero-field splitting effect from Mn(III), we can use eqs 7 and 8 to predict the ratio $\mathbf{D}_{III}/J$, $\mathbf{a}_{II}$ for Mn(II), and $\mathbf{a}_{III}$ for Mn(III). To simplify our analysis, we assume an isotropic Mn(II) intrinsic hyperfine tensor $\mathbf{a}_{II}$, $\mathbf{D}_{II}$ is taken to be zero, $\mathbf{D}_{III}$ for Mn(III) is taken as an axial tensor (defined as $D[S_z^2 - {}^1/_3 S(S+1)]$), and we approximate the observed rhombic hyperfine tensors for Mn(II) and Mn(III) in Table 2a as axial tensors with $A_{para} = A_z$, $A_{perp} = (A_x + A_y)/2$. The results are listed in Table 2b. For all the dimanganese(II,III) cases listed in Table 2, we find $D < 0$ and $\Delta a > 0$ for the Mn(III) ions. Both results lead to the conclusion that the electronic configuration for the Mn(III) ion in all these complexes is $d_{xy}^1 d_{yz}^1 d_{zx}^1 d_{z^2}^1$. Again we find that for complexes **3** and **4**, for which X-ray structural data are available,[3] this conclusion is consistent with the metrical data cited previously.

It's interesting to note that the intrinsic hyperfine anisotropy of the Mn(III) ion in MnCat(III,IV) is 38% smaller than in MnCat(II,III); $\Delta a = 52$ MHz (Table 1b) vs. $\Delta a = 83$ MHz (Table 2b), respectively. This indicates a larger asymmetry of the spin density surrounding the Mn(III) ion in the dimanganese(II,III) complexes than for dimanganese(III,IV) complexes. This appears to reflect an effect of the crystal field on the ground state orbital configuration rather than a consequence of different ligand covalencies, as can be seen by the lack of correlation with the isotropic ^{55}Mn hyperfine constants in Tables 1b and 2b.

On the other hand, Δa for Mn(III) in MnCat(III,IV) is close to, but slightly smaller than, that observed for the dimanganese(III,IV) complexes **1** and **2** (Table 1b; 56–65 MHz), which possess

Chart 1

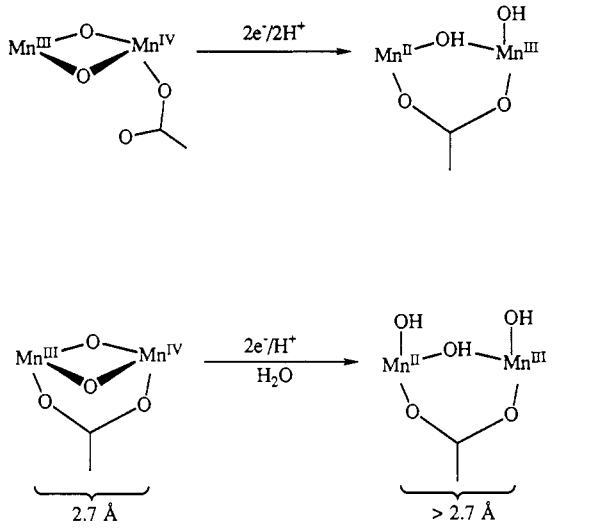

bis(μ-oxo) cores as their common structural feature. The closest similarity is to complex **1**, which possesses tetragonally extended ligand fields vs the trigonal ligand field imposed by the $HB(Pz)_3$ ligand in complex **2**. This empirical correlation suggests that MnCat(III,IV) may also have a bis(μ-oxo) bridge. This result is in agreement with the conclusion reached from the strong HDVV coupling,[8] and from recent Mn EXAFS studies of the *L. plantarum* catalase, which found the core structure to be comprised of $Mn(\mu\text{-}O)_2X_4$, X = O or N, with a Mn–Mn separation of 2.7 Å.[16]

By the same argument, the similar Δa values for MnCat(II,III) (83 MHz) and the dimanganese(II,III) complexes **3** and **4** (83 and 93 MHz, respectively, Table 2b) also suggests a similarity in the asymmetry of their spin densities. Complexes **3** and **4** possess $Mn(\mu\text{-}OR)(\mu\text{-}CH_3CO_2)_2N_3$ cores. Hence we suggest that MnCat(II,III) may possess the bridging core structure Mn(μ-OH)(μ-carboxylato)$_{1-2}$. This difference in bridging coordination modes between MnCat(III,IV) and MnCat(II,III) might become about as noted in Chart 1.

EPR "16-Line" Dogma. A "16-line" multiline EPR hyperfine pattern has long been regarded as a characteristic feature of the dimanganese(III,IV) oxidation state.[1,2] With our improved understanding of the influence of the zero-field splitting term and the greatly improved numerical fitting of the EPR spectra, it is appropriate to reexamine this issue here.

A 16-line EPR hyperfine pattern is obtained for the dimanganese(III,IV) oxidation state with two conditions: (1) The intrinsic hyperfine constant for Mn(III) is about the same as that of Mn(IV); (2) the spin projection of Mn(III) is twice that of Mn(IV). The first assumption is partially fulfilled by Mn(III) ions with an electronic configuration $d_{xy}^1 d_{yz}^1 d_{zx}^1 d_{z^2}^1$, in the sense that a_{perp} for Mn(III) is comparable to a_{iso} for Mn(IV). In the powder pattern EPR spectra of randomly oriented complexes in solution, it is the perpendicular component of the hyperfine tensor that determines most of the observed intensity, so assumption 1 is often found. A large deviation from the predicted 16-line pattern occurs when the second assumption breaks down. This can happen when the exchange interaction is not so strong. As we discussed in the previous section, the zero-field splitting term has a substantial influence on the observed hyperfine tensor in this case. This situation appears to be quite rare for dimanganese(III,IV) complexes, since the exchange interaction is usually large.

However, an apparent example of this situation has been reported recently for the Schiff base complex, $[Mn^{III}Mn^{IV}[2\text{-}OH\text{-}3,5\text{-}Cl_2\text{-}(SALPN)]_2(THF)]ClO_4$.[4] The previously reported X-band EPR spectrum is given in Figure 3a. It exhibits only 12 resolved peaks instead of the usual 16 peaks, with a 20–25% larger than normal peak-to-peak splitting of 100–110 G. In this complex the unusually long Mn–Mn separation (3.65 Å) and the

(14) Plaksin, P. M.; Stoufer, R. C.; Mathew, M.; Palenik, G. J. *J. Am. Chem. Soc.* **1972**, *94*, 2121–2122.

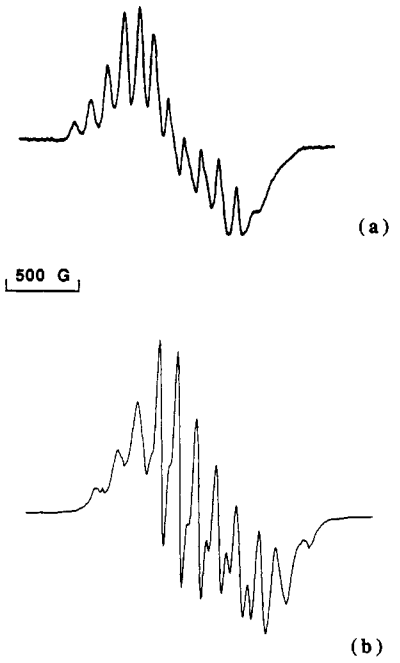

Figure 3. (a) X-band EPR spectrum of $Mn^{III}Mn^{IV}$[2-OH-3,5-Cl_2-(SALPN)]$_2$(THF)]ClO_4 in DMF at 20 K (reprinted with permission from ref 4). (b) Computer-generated spectrum using g_{perp} = 2.01, g_{para} = 1.93, and A_{III} = (−375, −375, −412) MHz, A_{IV} = (145, 145, 402) Mhz which correspond to intrinsic parameters a_{III} = (−230, −230, −150) MHz, D = −4 cm^{-1} (for Mn(III)), J = −10 cm^{-1}, a_{IV}(iso) = −230 MHz in eqs 4 and 5.

poor superexchange pathway (via a single alkoxide bridge) lead to weak magnetic exchange (J = −10 cm^{-1}), an order of magnitude smaller than commonly found in bis(μ-oxo)dimanganese(III,IV) complexes. In an attempt to explain this spectrum, we constructed effective hyperfine tensors for Mn(III) and Mn(IV) by using typical intrinsic hyperfine and zero-field splitting values in eqs 4 and 5. The parameters are given in the legend to Figure 3 and the simulated spectrum is given in Figure 3b. The spectrum has 11–13 lines with comparable overall breadth, splittings, and intensities to that of the experimental spectrum. The agreement is excellent considering that no attempt at least-squares fitting was possible, since a digitized spectrum was not available. Typical Mn(III) and Mn(IV) intrinsic magnetic parameters were used. This further demonstrates the capability of the theory in explaining a wide range of experimental data, including the case of weakly coupled ions.

Conclusions

We have examined ^{55}Mn magnetic hyperfine tensor data for dimanganese(III,IV) and dimanganese(II,III) systems possessing both strong and weak HDVV exchange coupling and both direct and transferred zero-field splittings. Highly accurate EPR spectral simulations derived from least-squares fitting analysis have been interpreted with this newly developed spin Hamiltonian.[13] This has enabled accurate determination of the Mn(III) electronic configuration, the magnetic hyperfine constants, and the D/J ratio. The intrinsic hyperfine constants for weakly coupled Mn ions have been shown to be reasonable, in contrast to the anomalous values deduced using the theory for strongly coupled spins.

New insight into the structure of the MnCat enzyme has also been learned. EPR spectral simulations positively identify the dimanganese(II,III) oxidation state in catalase. This is the first example of this oxidation state in any manganese protein. By comparison of the magnitude of hyperfine anisotropy of Mn(III) ions in the two mixed valence oxidation states of MnCat a large increase in the spin density asymmetry is observed for MnCat-(II,III) which indicates a probable change in the ligand coordination. Core conversion from $[Mn_2(\mu\text{-}O)_2(carboxylate)_{0-1}]^{3+/2+}$ to a $[Mn_2(\mu\text{-}OH)(carboxylate)_{1-2}]^{3+/2+}$ (Chart 1) upon reduction would be consistent with this change in spin density.

These results offer a plausible explanation for why there is a 10^{12} slower rate constant for dismutation of peroxide by MnCat-(III,IV) compared to the MnCat(II,II) oxidation state involved in the physiological activity.[8,17] In MnCat(III,IV) the combined consequences of having strong Mn–O bonding within the Mn-(μ-O)$_2$ core, six-coordinate Mn ions which exhibit strong valence trapping, and restricted access to the active site containing at most one labile solvent molecule located within 4 Å to the Mn_2-(μ-O)$_2$ core[15] insure that turnover of MnCat(III,IV) by oxidation of a peroxide molecule will be a slow process. This suggests that reduction may occur by an outer sphere electron transfer process for MnCat(III,IV), or be limited by slow ligand exchange. Because the antibonding d_{z^2} electron of Mn(III) is predicted to be orthogonal to the μ-O atoms of the $Mn_2(\mu\text{-}O)_2$ rhombus, slow ligand exchange is expected. By contrast, considerably faster ligand substitution reactions are observed for MnCat(II,II).[8b,d] Similarly, the rate of reduction of MnCat(II,III) by peroxide is orders of magnitude faster than found for MnCat(III,IV).[8,17] The proposed loss of the strong ligand field from (μ-O)$_2$ depicted in Chart 1 offers a simple explanation for these kinetic differences.

Our future studies will focus on determining the orbital configuration of Mn(III) ions in other enzymes and catalysts and correlating this with differences in the reactivity of ligand atoms bound at sites directed either towards or in between the antibonding d_σ orbital.

Acknowledgment. This research was partially supported by NIH Grant GM 39932. M.Z. acknowledges an ARCO summer research fellowship. G.C.D. thanks the Chemistry Dept. of Princeton University for interim research support. We thank Dr. V. Pecoraro for a copy of Figure 3a, Mr. P. J. Pessiki for sample preparation, and Dr. N. Kitajima for sharing unpublished EPR data.

(15) Khangulov, S. V.; Sivaraja, M.; Barynin, V. V.; Dismukes, G. C. *Biochemistry* **1993**, *32*, 4912–4924.
(16) Waldo, G. S.; Yu, S.; Penner-Hahn, J. E. *J. Am. Chem. Soc.* **1992**, *114*, 5869–5870.
(17) Dismukes, G. C. Polynuclear Manganese Enzymes. In *Bioinorganic Catalysis*; Reedijk, J., Ed.; Marcel-Dekker: Amsterdam, 1992; pp 317–346.